



This is the accepted manuscript made available via CHORUS, the article has been published as:

Unusual structural evolution in KCuF_3 at high temperatures by neutron powder diffraction

Luke G. Marshall, Jianshi Zhou, Jianzhong Zhang, Jiantao Han, Sven C. Vogel, Xiaohui Yu, Yusheng Zhao, M. T. Fernández-Díaz, Jinguang Cheng, and John B. Goodenough

Phys. Rev. B **87**, 014109 — Published 22 January 2013

DOI: [10.1103/PhysRevB.87.014109](https://doi.org/10.1103/PhysRevB.87.014109)

The unusual structural evolution in KCuF_3 by neutron powder diffraction at high temperatures

Luke G. Marshall¹, Jianshi Zhou^{1*}, Jianzhong Zhang², Jiantao Han², Sven C. Vogel², Xiaohui Yu², Yusheng Zhao^{2,3}, M.T. Fernández-Díaz⁴, Jinguang Cheng¹, John B. Goodenough¹

¹ The Materials Science and Engineering Program and Texas Materials Institute, University of Texas at Austin, Austin, TX 78712

² LANSCE Division, Los Alamos National Laboratory, Los Alamos, NM 87545, USA

³ Department of Physics and Astronomy, University of Nevada, Las Vegas, NV 89154

⁴ Institute Laue-Langevin (ILL) 156X, F-38042 Grenoble Cedex 9, France

Abstract

High-resolution neutron powder diffraction has been performed to study the structural evolution of the perovskite KCuF_3 at temperatures up to 900 K. Results of the Rietveld refinement reveal an unusual site distortion that increases as temperature increases. In contrast to the widely accepted assumption that a cooperative Jahn-Teller transition may occur at 800 K, no phase transition was observed up to 900 K. We have made a comparative study of the Jahn-Teller distortion in fluorides and oxides with variables such as temperature, pressure, and the dilution by non-Jahn-Teller active ions in these compounds.

Introduction

Orbital degeneracy on Cu^{2+} (d^9) ions in the cubic crystal field makes perovskite KCuF_3 a Jahn-Teller (JT) active system. The perovskite KCuF_3 has been of interest for the symmetry of its orbital ordering and low-dimensional magnetism since Kugel and Khomskii used the compound as their prototypical system in a seminal work showing that orbital order can be induced via purely electronic superexchange interactions [1]. The Kugel-Khomskii (KK) model has been widely used in calculations for the spin dynamics and spin ordering at $T_N \sim 38$ K in KCuF_3 [2 – 9]. In the KK model, the e electron occupies the x^2-z^2/y^2-z^2 orbital, which produces two short and four long Cu-F bonds in the tetragonal structure, corresponding to the $60^\circ/300^\circ$ directions in the (Q_2, Q_3) space of orthorhombic vibrational modes. The cooperative Jahn-Teller (cJT) distortion

of the CuF_6 octahedra makes KCuF_3 tetragonally distorted at room temperature [10-12]; this is in contrast to most other non-JT active perovskite fluorides KMF_3 ($M = \text{Mg, V, Mn, Fe, Co, Ni, Zn}$) which all have the simple cubic perovskite structure [13]. The cJT ordering temperature of about 800 K has been cited in several relevant publications [3, 10, 11, 14, 15]. In a calculation using the local-density approximation + dynamical mean-field theory, however, Pavarini *et al.* [12] have shown that superexchange interactions which induce the orbital ordering with $60^\circ/300^\circ$ modes, can cause an orbital order-disorder transition at $T_{\text{KK}} \sim 350$ K, far below the $T_{\text{JT}} \sim 800$ K reported in the literature. In order to resolve this discrepancy, we have first studied the accuracy and reliability of experiments that have shown a cJT transition in the literature. Based on the data available to us, there is no direct evidence that cJT transition takes place at high temperatures. An early neutron-diffraction study of KCuF_3 [14] was focused on the magnetic structure at low temperatures and no data about the structural evolution as a function of temperature were given. The most cited report regarding the orbital order-disorder transition in KCuF_3 is a study that used resonant X-ray scattering [3]. The scattering cross section in the orbitally ordered phase includes information about the orbital ordering parameter (OP). The entire experiment was performed at cryogenic temperatures. The authors have observed a steeper rise of the orbital OP on cooling through T_{N} , which was thought to signal a strong spin-orbital interaction. By using $T_{\text{OO}} = 800$ K as a fitting parameter, the authors were able to fit the observed OP(T) curve at low temperatures. By using a short wave length synchrotron radiation ($\lambda = 0.29513$ Å), Ghigna et al [16] have studied the structural evolution as a function of temperature for a solid solution $\text{KCu}_{1-x}\text{Mg}_x\text{F}_3$. Although the study did not give the local structural distortion, the authors have predicted a $T_{\text{JT}} \approx 1350$ K for the parent phase KCuF_3 by extrapolating the tetragonal/cubic phase boundary to $x=0$. Neutron powder diffraction at high temperatures is a direct and conclusive experiment to address this long-standing issue. In this paper, we report the result of high-resolution neutron diffraction from room temperature up to 900 K. The outcome of our experiment is quite surprising, and it forces us to reconsider existing models for KCuF_3 .

Experimental details

Single crystals of KCuF_3 have been grown by following the procedure described in Ref. [2]. We have pulverized crystals for neutron powder diffraction (NPD). The powder sample was first checked by laboratory X-ray powder diffraction. High-temperature neutron time-of-flight

diffraction experiments were performed at the Los Alamos Neutron Science Center (LANSCE) on the HIPPO (High-Pressure Preferred Orientation) instrument [17, 18]. The sample was loaded in an 8.5 mm inner-diameter Vanadium can of 0.15 mm wall thickness, and NPD measurements were taken at temperatures up to 900 K with 1 hour count times at each temperature enabling crystal structure analysis, including the refinement of the atomic positions and isotropic thermal motion parameters. Since a small amount CuO was detected after heating up the sample to 950 K in an Ar atmosphere in the previous experiment [19], neutron powder diffraction was kept below 900 K. 42 out of the 50 HIPPO detector panels are usable with the furnace; the panels are located at nominal diffraction angles of 140, 120, 90, 60 and 40 degrees. The vanadium heating elements and heat shields of the ILL-type furnace were utilized for this experiment. The furnace was evacuated to $<10^{-5}$ Torr. The NPD patterns were analyzed by the Rietveld method with the EXPGUI for GSAS software [20, 21]. The powder sample recovered after 900 K in this experiment was compared with a fresh powder sample by room-temperature neutron powder diffraction at the beamline D2B in ILL. No obvious change in chemistry has been detected.

Results and Discussion

X-ray and neutron diffraction patterns (NPD) were refined with the structural model in space group $I4/mcm$ from Ref. 22; the fitting quality is reasonable, see Fig. 1 for the NPD and fitting results. We have also attempted to refine the NPD at room temperature with the monoclinic $P2_12_12_1$ structural model used in an earlier neutron diffraction study, but no superlattice peaks were found that could not be indexed by the tetragonal cell [23]. We used the tetragonal model in refining all neutron diffraction patterns at different temperatures; the results from the refinements are listed in Tables 1 and ref.24. Instead of a simple cubic cell as with other non-JT active perovskites KMF_3 , the cooperative JT distortion of the CuF_6 octahedra enlarges the lattice parameters in the basal plane, and the out-of-phase arrangement between layers along the c axis doubles the primary cell in this direction [23]. In contrast to the expectation that the cJT distortion will vanish above 800 K [3, 10, 11, 14, 15], the temperature dependence of lattice parameters of Fig. 2 indicates that the same unit cell at room temperature, and therefore the cJT phase, remains stable up to 900 K, the highest temperature in this study. This stunning result has been further confirmed by the refinement results. In another JT active fluoride $KCrF_3$, the

tetragonal cell collapses into a cubic cell at $T_{JT} = 970$ K [25]. A similar lattice parameter change has also been found in a JT active perovskite oxide LaMnO_3 [26]. The cooperative orbital ordering places $c/\sqrt{2} > a$ found in a typical orthorhombic cell like GdFeO_3 into $c/\sqrt{2} < a$ [27]. At $T > T_{JT}$, a pseudo cubic phase has been found in LaMnO_3 . A dramatic difference in the structural evolution for the JT distortion phase as a function of temperature between the oxide and the fluorides is that a progressive collapse of the orthorhombic cell is clearly visible at $T < T_{JT}$ in the oxide whereas the collapse of the tetragonal cell in KCrF_3 appears to be abrupt. However, the separation between $a/\sqrt{2}$ and $c/2$ in KCuF_3 is even enlarged as temperature increases, which is opposite to that in the known JT systems. A different influence of thermal fluctuations on the cJT distortion between oxides and fluorides is made evident by Rietveld refinements.

Rietveld refinements reveal further information about the local structural distortion in KCuF_3 . The JT effect plus the intrinsic structural distortion lead to a long, a medium, and a short Cu-F bond at a CuF_6 octahedron [19]. Fig. 3 shows that the bonding split remains and becomes significantly larger as temperature increases. These observations are in sharp contrast to the high-temperature behavior superimposed in the same plot for the JT active perovskites LaMnO_3 and KCrF_3 in which the split of M-O(F) bond lengths gradually converges as T_{JT} is approached from low temperatures [25, 26]. One may be curious about the occupancy rate, especially for F2 ions; the occupancy rate drops slightly from 98% to 90% with increasing temperature. However, our result showing no obvious change in chemistry for the sample recovered should ease this concern.

Rigid octahedra would occur only in the simple cubic perovskite structure $Pm-3m$. Octahedral-site rotations in all perovskite structures with subgroup symmetries also lead to octahedral-site distortions, *i.e.* a bond-length split. The JT distortion in the JT active perovskites enlarges the bond-length split significantly. The bond-length splitting in turn reflects the orbital occupation. In most cases, the intrinsic structural distortions cause a mixture of two e orbitals $3x^2-r^2$ and y^2-z^2 or $3y^2-r^2$ and z^2-x^2 for strong JT ions with degenerate e orbitals. It is most convenient to plot the octahedral-site distortion in the orthorhombic vibrational modes (Q_2 , Q_3) of Fig. 4. Similar to the orbital occupation in LaMnO_3 , the bond length split of KCuF_3 at room temperature does not correspond to occupying the $3x^2-r^2$ ($3y^2-r^2$) orbital. Instead, the orbital mixture of $3x^2-r^2$ and y^2-z^2

places KCuF_3 at a spot away from the 120° direction. The magnitude of the site distortion measured by $\rho = (Q_2^2 + Q_3^2)^{1/2}$ is comparable to other JT active perovskites LaMnO_3 and KCrF_3 . It is interesting to study from this plot how the JT distortion evolves as a function of temperature, pressure, and the dilution by non-JT ions and to compare this evolution with that of other JT active perovskites.

The JT distortion in KCuF_3 can be reduced by substituting for Cu^{2+} a non-JT ion like Mg^{2+} [16,27]. In the polar plot, the distortion is reduced following a pathway with an arc towards the 120° direction as the dilution concentration increases. The pressure effect on KCuF_3 , as demonstrated in a previous study [19], also reduces the JT distortion. It is interesting to notice that the pathways for reducing the JT distortion in KCuF_3 by dilution with Mg^{2+} and hydrostatic pressure are nearly identical. In comparison, these two methods are also very efficient to reduce the JT distortion in LaMnO_3 . In this case, the non-JT ion Ga^{3+} is used as the dilution ion [28]. Whereas the pathways following these two routes look identical, i.e. an arc towards the Q_2 axis, they are different from those found for the fluoride perovskite. It is still not clear for us whether to attribute the difference of the pathway to the structural symmetry, i.e. the orthorhombic versus the tetragonal phase, or to the chemistry, i.e. oxide versus fluoride.

We now turn to the temperature effect on the JT distortion. Thermal fluctuations and the long-range cooperative orbital order due to the JT effect are two competing forces. Orbital ordering melts at a sufficiently high temperature, $T_{\text{JT}} = 750$ K for LaMnO_3 [26]. Note that for LaMnO_3 , the pathway in Fig.4 for reducing the JT distortion is nearly the same for increasing temperature as it is by dilution or placing the sample under high pressure. We have taken a JT active fluoride KCrF_3 for comparison. Raising temperature does not influence the JT distortion in KCrF_3 as dramatically as it does in LaMnO_3 before the cooperative orbital order collapses at 970 K. There is no significant difference of the JT distortion at room temperature between two fluoride perovskites, KCrF_3 and KCuF_3 . However, as shown in Fig. 4, the high-temperature behavior of the JT distortion in KCuF_3 is fundamentally different from that in KCrF_3 and in oxides as well. The observation of increased JT distortion as temperature increases is against our common knowledge about this type of phase transition; it means that the long-range cooperative orbital ordering due to the JT effect remains stable up to a temperature where the compound is melted or

decomposes. The robust JT distortion found in KCuF_3 and the negligible temperature dependence of the JT distortion found in KCrF_3 call for a systematic study for the intrinsic structural distortion in fluoride perovskites as there has been for oxide perovskites [28]. The site distortion in non-JT active fluorides may become more severe as temperature increases. This effect could offset or even over balance the reduction of the JT distortion as temperature increases in KCrF_3 and KCuF_3 .

Conclusion

The fluoride perovskite KCuF_3 exhibits an unusual structural evolution; the site distortion due to the Jahn-Teller effect increases as temperature increases. We have made an extensive comparative study of other Jahn-Teller active oxide and fluoride perovskites. They all show that the JT distortion is reduced progressively by substituting non-JT active ions for the JT active ions or under hydrostatic pressure, although the oxide and the fluoride follow slightly different pathways on reduction of the JT distortion. The temperature effect on the JT distortion is sharply different for the oxide and fluorides. The long-range cJT distortion in LaMnO_3 reduces as temperature increases and eventually vanishes at $T_{\text{JT}} = 750$ K, whereas the temperature effect on the cJT distortion is negligible in KCrF_3 until it collapses abruptly at $T_{\text{JT}} = 970$ K; the JT distortion increases in KCuF_3 as temperature increases to 900 K. The temperature dependence suggests that the cJT transition in KCuF_3 would not occur at any temperature below the decomposition temperature.

Acknowledgements

This work was supported by NSF (DMR 0904282, DMR 1122603) and the Robert A Welch foundation (Grant F-1066).

* jszhou@mail.utexas.edu

Tables and Figures

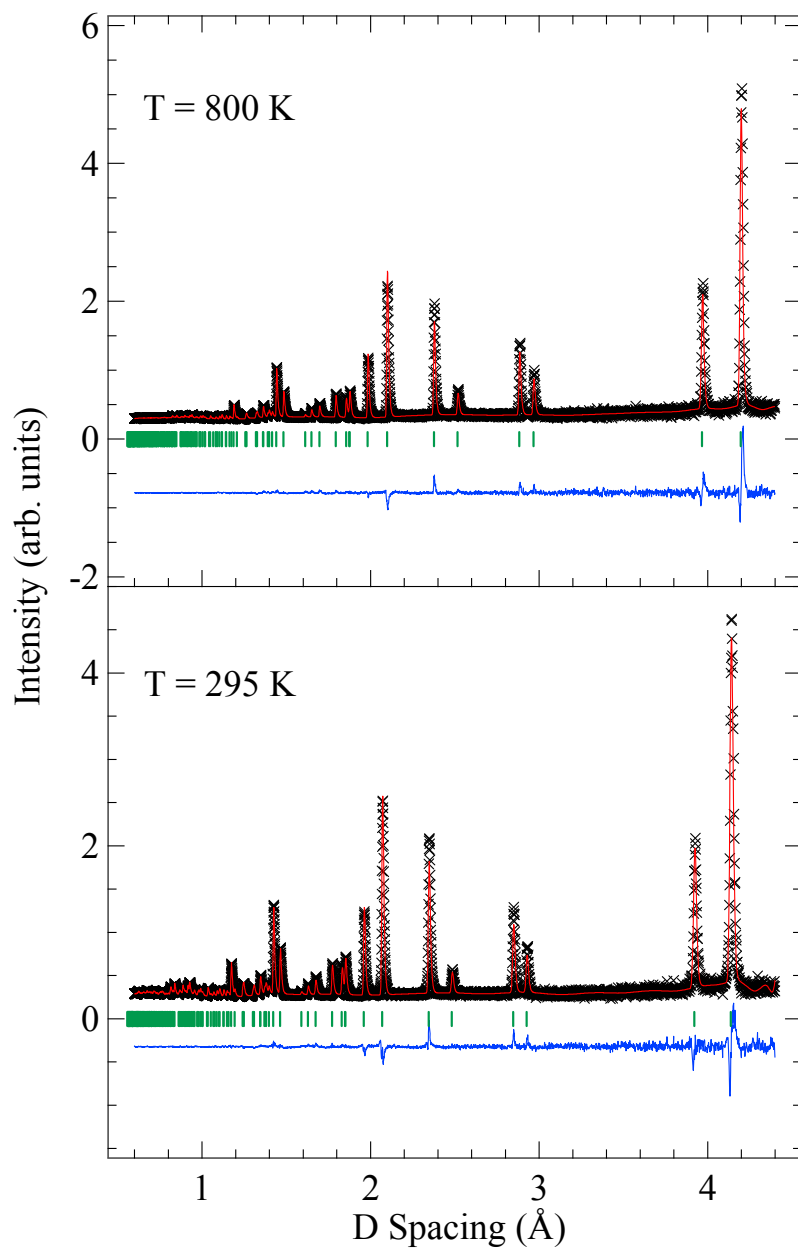


Fig. 1 (Color online) NPD diagrams for ambient temperature and 800 K, fitted to the model described in the text in the $I4/mcm$ space group. Observed profile (circles), calculated (full line), and difference (down) profiles, with the allowed Bragg reflections as vertical marks.

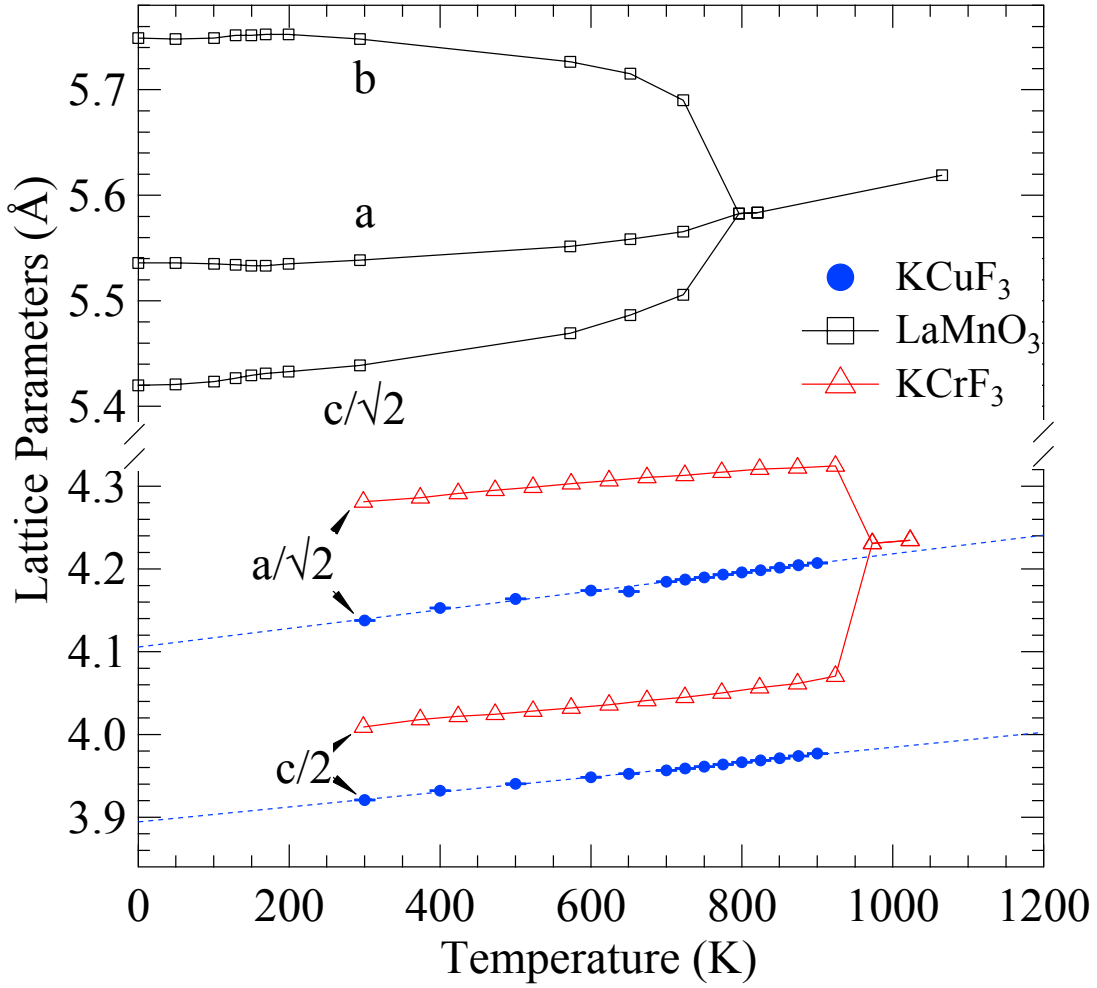


Fig. 2 (Color online) **(i)** Temperature dependence of the lattice parameters of LaMnO₃ through the cJT transition temperature $T_{JT} \sim 750$ K from Ref. 25. **(ii)** Temperature dependence of the primary cell lattice parameters of KCrF₃ [25] and KCuF₃ through their expected JT distortions. The error bars are smaller than the symbols. Structural phase transitions are usually preceded by a deviation from the cell parameters trend line, as seen with LaMnO₃[26]; however, no such deviation is observed for KCrF₃ until the lattice parameters collapse to pseudo-cubic at $T_{JT} \sim 970$ K. The JT distortion increases with temperature for KCuF₃ through 900 K, with no indication of the occurrence of a structural phase transition before its decomposition.

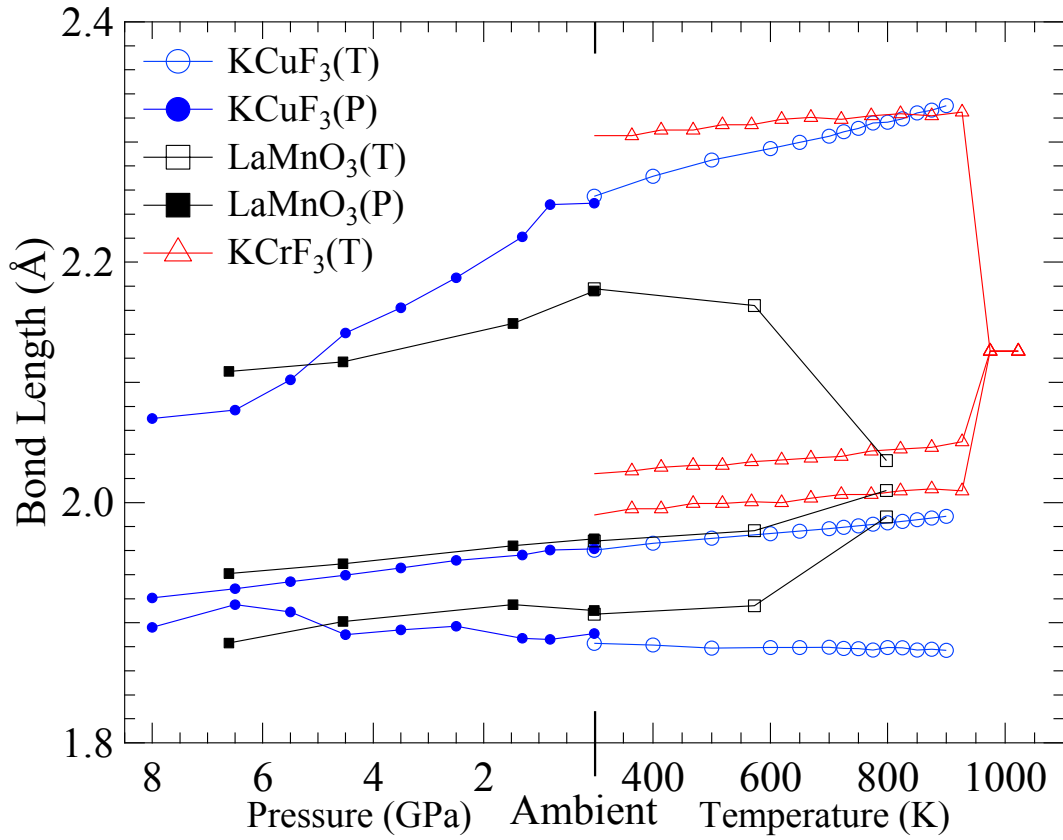


Fig. 3 (Color online) The pressure and temperature dependence of the bonds in the MnO_6 [26, 29], CrF_6 [25], and CuF_6 octahedra from Ref. 19 and this work. The error bars are smaller than the symbols. LaMnO_3 and KCrF_3 show a collapse of their long, medium and short bonds into degenerate lengths after passing through their T_{JT} at 750 K and 970 K, respectively. KCuF_3 shows no indication of this through the expected Jahn-Teller distortion onset temperature $T_{\text{JT}} \sim 800$ K. Under high pressure, the JT distortion of both LaMnO_3 and KCuF_3 is suppressed.

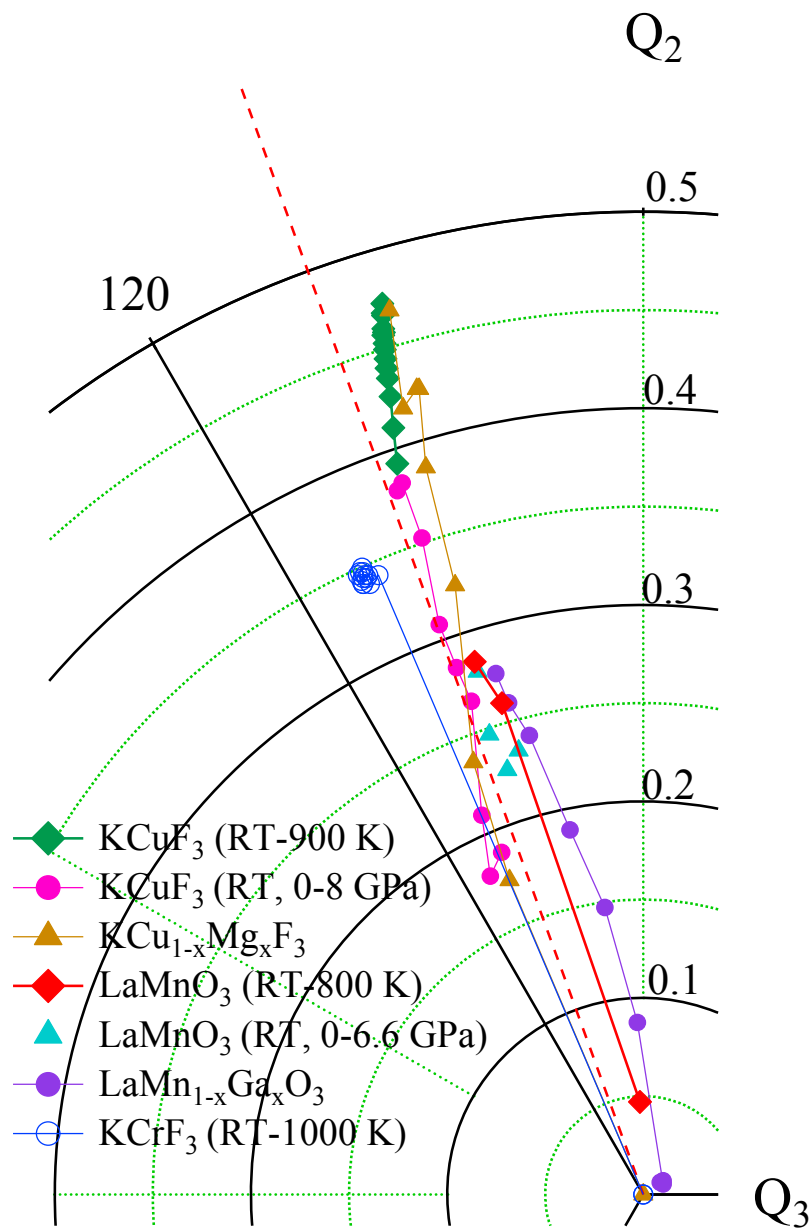


Fig. 4 (Color online) A quarter of the polar plot of the site distortion of KCuF_3 , KCrF_3 , and LaMnO_3 as a function of temperature, pressure, and dilution by non-JT ions. Data in this plot are

from this work, and Refs. 19, 27, 26, 30, 28, 25 in the order they appear.

Table 1: Temperature evolution of the interatomic distances (\AA) for KCuF_3 , from NPD.

T (K)	300	400	500	600	650	700	725	750	775	800	825	850	875	900
K-F1 (x4)	2.92574(6)	2.93640(7)	2.94423(7)	2.95139(7)	2.95498(8)	2.95878(8)	2.96075(8)	2.96267(8)	2.96483(8)	2.96672(8)	2.96874(7)	2.97084(7)	2.97288(7)	2.97494(7)
K-F2 (x8)	2.85609(7)	2.86615(8)	2.87354(9)	2.8802(1)	2.8836(1)	2.8872(1)	2.8892(1)	2.8911(1)	2.8933(1)	2.8950(1)	2.8971(1)	2.8993(1)	2.9013(1)	2.9035(1)
Cu-F1 (x2)	1.96028(5)	1.96609(5)	1.97022(5)	1.97412(6)	1.97615(6)	1.97832(6)	1.97948(6)	1.98063(6)	1.98189(6)	1.98309(6)	1.98439(6)	1.98572(6)	1.98704(7)	1.98843(7)
Cu-F2 (x2)	1.8829(9)	1.881(1)	1.879(1)	1.879(1)	1.879(1)	1.879(1)	1.879(1)	1.878(1)	1.877(1)	1.879(1)	1.879(1)	1.8771(14)	1.878(1)	1.877(1)
Cu-F2' (x2)	2.2548(9)	2.271(1)	2.285(1)	2.295(1)	2.300(1)	2.305(1)	2.308(1)	2.311(1)	2.316(1)	2.316(1)	2.319(1)	2.324(1)	2.326(1)	2.330(1)

References

- [1] K.I. Kugel, D.I. Khomskii, *Sov. Phys. Usp.* 25 (1982) 231.
- [2] R. Caciuffo, L. Paolasini, A. Sollier, P. Ghigna, E. Pavarini, J. van den Brink, M. Altarelli, *Phys. Rev. B* 65 (2002) 174425.
- [3] L. Paolasini, R. Caciuffo, A. Sollier, P. Ghigna, M. Altarelli, *Phys. Rev. Lett.* 88 (2002) 106403.
- [4] M. Takahashi, J.-I. Igarashi, *Physica B* 329–333 (2003) 870.
- [5] A.I. Liechtenstein, V.I. Anisimov, J. Zaanen, *Phys. Rev. B* 52 (1995) R5467.
- [6] M.V. Eremin, J. Deisenhofer, I. Leonov, M.V. Eremin, Ch. Kant, P. Ghigna, F. Mayr, V.V. Iglamov, V.I. Anisimov, D. van der Marel, *Phys. Rev. Lett.* 101 (2008) 147601.
- [7] I. Leonov, N. Binggeli, Dm. Korotin, V.I. Anisimov, N. Stojic, D. Vollhardt, *Phys. Rev. Lett.* 101 (2008) 096405.
- [8] M.D. Towler, R. Dovesi, V.R. Saunders, *Phys. Rev. B* 52 (1995) 10150.
- [9] N. Binggeli, M. Altarelli, *Phys. Rev. B* 70 (2004) 085117.
- [10] A. Okazaki, *J. Phys. Soc. Jpn.* 26, 870 (1969).
- [11] M. Hidaka, T. Eguchi, and I. Yamada, *J. Phys. Soc. Jpn.* 67, 2488 (1998).
- [12] E. Pavarini, E. Koch, A.I. Lichtenstein, *Phys. Rev. Lett.* 101 (2008) 266405.
- [13] F. Aguado, F. Rodriguez, S. Hirai, J.N. Walsh, A. Lennie, A.T. Redfern, *High Pressure Res.* 28 (2008) 539.
- [14] M.T. Hutchings, E.J. Samuelsen, G. Shirane, K. Hirakawa, *Phys. Rev.* 188 (1969) 919.
- [15] J.C.T. Lee, S. Yuan, S. Lal, Y. Il Joe, Y. Gan, S. Smadici, K. Finkelstein, Y. Feng, A. Ruydi, P.M. Goldbart, S.L. Cooper, P. Abbamonte, *Nature Physics* 8, 63–66 (2012).
- [16] P. Ghigna, M. Scavini, C. Mazzoli, M. Bruelli, C. Laurenti, and C. Ferrero, *Phys. Rev. B* 81, 73107 (2010)
- [17] H.-R. Wenk, L. Lutterotti, and S. Vogel, *Nucl. Instrum. Methods Phys. Res. A* **515**(3), 575–588 (2003).
- [18] S. Vogel, C. Hartig, L. Lutterotti, R.B. von Dreele, H.-R. Wenk, and D.J. Williams, *Powder Diffr.* **19**, 65–68 (2004)
- [19] J.-S. Zhou, J.A. Alonso, J.T. Han, M.T. Fernández-Díaz, J.-G. Cheng, J.B. Goodenough, *J. Fluorine Chem.* 132 (2011) 1117–1121.
- [20] B. H. Toby, *J. Appl. Cryst.* (2001). 34, 210-213
- [21] A.C. Larson, and R.B. Von Dreele, Los Alamos National Laboratory Report LAUR 86-748 (1994).
- [22] R.H. Buttner, E.N. Maslen, N. Spadaccini, *Acta Crystallogr. B* 46 (1990) 131.
- [23] M. Hidaka, T. Eguchi, I. Yamada, *J. Phys. Soc. Jpn.* 67 (1998) 2488.

- [24] See Supplemental Materials at
- [25] S. Margadonna, G. Karotsis, *J. Mater. Chem.* **17**, 2013-2020 (2007).
- [26] J. Rodriguez-Carvajal, M. Hennion, F. Moussa, A.H. Moudden, L. Pinsard, A. Revcolevschi, *Phys. Rev. B* **57** (1998) R3189.
- [27] P.C. Burns, F.C. Hawthorne, A.M. Hofmeister, S.L. Moret, *Phys. Chem. Minerals* **23**, 141-150 (1996).
- [28] J.-S. Zhou, J.B. Goodenough, *Phys. Rev. B* **77** (2008) 172409.
- [29] J.-S. Zhou, J.B. Goodenough, *Phys. Rev. B* **77** (2008) 132104.
- [30] L. Pinsard-Gaudart, J. Rodriguez-Carvajal, A. Daoud-Aladine, I. Goncharenko, M. Medarde, R.I. Smith, A. Revcolevschi, *Phys. Rev. B* **64** (2001) 064426.